PROCEEDINGS OF SCIENCE

ZH production in the SMEFT from gluon fusion

Marion O. A. Thomas[a,*]

[a] *Dept. of Physics and Astronomy, University of Manchester, Oxford Road, Manchester M13 9PL, UK*

E-mail: marion.thomas@manchester.ac.uk

We study in a systematic way ZH production in the Standard Model Effective Field Theory framework. We first calculate analytical expressions for the helicity amplitudes of the gluon-induced channel with up to one insertion of a CP-even dimension-6 operator. We then study the high-energy behaviour of the helicity amplitudes in order to identify to which operators $gg \to ZH$ is most sensitive. Additionally, we conduct a phenomenological analysis of ZH production, considering both quark and gluon initial states. We find that for some third-generation operators, the loop-induced channel provides competitive sensitivity to constraints obtained from top quark production processes. Finally we consider CP-odd operators and extend the `SMEFTatNLO` implementation to include the CP-violating top Yukawa operator, and present preliminary results of its impact on gluon-induced ZH production.

ArXiv ePrints: 2306.09963, 2411.00959

12th Large Hadron Collider Physics Conference (LHCP2024)
3-7 June 2024
Boston, USA

*Speaker

PoS(LHCP2024)129

1. Introduction

At the LHC, ZH production is dominated by the tree-level quark-induced channel. Nonetheless, the gluon fusion channel is highly relevant to study and constrain Higgs and top quark properties as it is mediated by top quark loop diagrams. In particular, this process can be used to probe deviations from the Standard Model in the top, Higgs, and electroweak sectors using the Standard Model Effective Field Theory (SMEFT) framework. Formally, the SMEFT extends the SM Lagrangian to higher dimensional operators with an expansion in energy:

$$\mathcal{L}_{\text{SMEFT}} = \mathcal{L}_{\text{SM}} + \sum_{d=5}^{\infty} \sum_{k} \frac{c_k}{\Lambda^{d-4}} O_k^{(d)} \tag{1}$$

where each operator $O_k^{(d)}$ has energy dimension (d), c_k is the corresponding dimensionless Wilson coefficient (WC), and the series converges as long as the typical energy of the process obeys $E/\Lambda \ll 1$. We focus on the dimension-six operators and use the Warsaw basis [1] along with a $\mathrm{U}(2)_q \times \mathrm{U}(3)_d \times \mathrm{U}(2)_u \times (\mathrm{U}(1)_\ell \times \mathrm{U}(1)_e)^3$ flavour assumption. In these proceedings, we focus on the third-generation quark operators entering in ZH production, as well as on contact Higgs-gluon interactions, and the relevant operators are presented in Table 1.

O_i	c_i	Definition	O_i	c_i	Definition
$O_{\varphi G}$	$c_{\varphi G}$	$\left(\varphi^\dagger\varphi - \frac{v^2}{2}\right) G^{\mu\nu}_A G^A_{\mu\nu}$	$O_{\varphi t}$	$c_{\varphi t}$	$i\left(\varphi^\dagger \overleftrightarrow{D}_\mu \varphi\right)\left(\bar{t}\,\gamma^\mu\, t\right)$
O_{tG}	c_{tG}	$g_s \left(\bar{Q}\sigma^{\mu\nu} T_A\, t\right) \tilde{\varphi}\, G^A_{\mu\nu}$ + h.c.	$O^{(1)}_{\varphi Q}$	$c^{(1)}_{\varphi Q}$	$i\left(\varphi^\dagger \overleftrightarrow{D}_\mu \varphi\right)\left(\bar{Q}\,\gamma^\mu\, Q\right)$
$O_{t\varphi}$	$c_{t\varphi}$	$\left(\varphi^\dagger\varphi - \frac{v^2}{2}\right) \bar{Q}\, t\, \tilde{\varphi}$ + h.c.	$O^{(3)}_{\varphi Q}$	$c^{(3)}_{\varphi Q}$	$i\left(\varphi^\dagger \overleftrightarrow{D}_\mu \tau_I \varphi\right)\left(\bar{Q}\,\gamma^\mu\, \tau^I Q\right)$
			$O^{(-)}_{\varphi Q}$	$c^{(-)}_{\varphi Q}$	$c^{(1)}_{\varphi Q} - c^{(3)}_{\varphi Q}$

Table 1: Dimension-6 operators O_i and their associated Wilson Coefficients c_i entering in $gg, q\bar{q} \to ZH$ and considered in these proceedings. We follow the notation introduced in [2].

2. Growing amplitudes in $gg \to ZH$

We start by considering the impact of CP-even SMEFT operators on the helicity amplitudes of the gluon-induced channel. Representative diagrams are shown in Fig. 1. There are 12 possible helicity combinations for $gg \to ZH$, but using the Bose symmetry of the initial state gluons and the CP properties of the operators considered leads to 5 independent helicity combinations. We calculated analytical expressions for the helicity amplitudes of $gg \to ZH$ with up to one insertion of a dimension-6 SMEFT operator in Wolfram Mathematica using the FeynCalc [3–5], FeynHelpers [6], Package-X [7] and FeynArts [8] packages. We then studied the high-energy behaviour of the amplitudes in order to establish to which operators loop-induced ZH production is most sensitive to, and in which helicity configurations. The growing SMEFT amplitudes are given in Tables 2 and 3, and are given in terms of the vector and axial-vector parts of the SM $t\bar{t}Z$ vertex

which can be expressed as:

$$eZ_\mu \bar{t}\gamma^\mu (c_V + c_A\gamma^5)\, t \qquad \text{where } c_V = \frac{1}{4c_w s_w}\left(1 - \frac{8s_w^2}{3}\right),\ c_A = \frac{-1}{4c_w s_w} \tag{2}$$

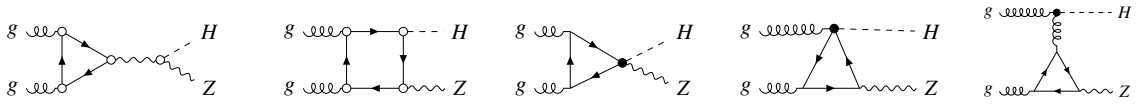

Figure 1: Diagram topologies that enter in the computation of $gg \to ZH$ in the SMEFT at one-loop for the WCs considered in these proceedings. The empty dots represent couplings that could be either SM-like or modified by dimension-6 operators. The filled dots represent vertices generated only by dimension-6 operators. Only one insertion of dimension-6 operators is allowed per diagram.

$\lambda_{g_1}, \lambda_{g_2}, \lambda_H, \lambda_Z$	SM	O_{tG}	$O_{\varphi G}$
$+,+,0,+$	$\frac{1}{\sqrt{s}}\log^2\left(\frac{s}{m_t^2}\right)$	$\sqrt{s}\,\frac{m_t\, e\, g_s^2\, c_A\, c\theta}{2\,\pi^2\sqrt{1-c\theta^2}}\log\left(\frac{s}{m_t^2}\right)$	–
$+,+,0,-$	$\frac{1}{s^{3/2}}\log^2\left(\frac{s}{m_t^2}\right)$	$\sqrt{s}\,\frac{m_t\, e\, g_s^2\, c_A\, c\theta}{4\,\pi^2\sqrt{1-c\theta^2}}\log^2\left(\frac{s}{m_t^2}\right)$	–
$+,+,0,0$	$\frac{1}{s}\log^2\left(\frac{s}{m_t^2}\right)$	$\frac{m_t(m_Z^2(1+c\theta^2)-m_t^2(5-c\theta^2))\, e\, g_s^2\, c_A}{2\sqrt{2}\,\pi^2\, m_Z\,(1-c\theta^2)}\log^2\left(\frac{s}{m_t^2}\right)$	$\frac{m_t^2\, v\, e\, g_s^2\, c_A}{\pi^2\, m_Z\,(1-c\theta^2)}\log^2\left(\frac{s}{m_t^2}\right)$
$+,-,0,+$	$\frac{1}{\sqrt{s}}\log^2\left(\frac{s}{m_t^2}\right)$	$\sqrt{s}\,\frac{m_t\, e\, g_s^2\, c_A}{4\,\pi^2}\, f_1(c\theta)$	–
$+,-,0,0$	s^0	$s\,\frac{m_t\, e\, g_s^2\, c_A\, c\theta}{2\sqrt{2}\,\pi^2 m_Z}$	$\frac{m_t^2\, v\, e\, g_s^2\, c_A\, c\theta}{\pi^2\, m_Z\,(1-c\theta^2)}\log^2\left(\frac{s}{m_t^2}\right)$

Table 2: High energy behaviour of the $gg \to ZH$ helicity amplitudes in the SM and with modified top-gluon and Higgs-gluon interactions. The cosine and the sine of the weak angle are represented by c_w and s_w respectively. For readability we have defined $f_1(c\theta) = \left[1 - 3c\theta^2 + 2c\theta^3 + (1-c\theta^2)\left(\log(\frac{1+c\theta}{2}) + i\pi\right) + (1 + c\theta)\log(\frac{1+c\theta}{2})(\log(\frac{1+c\theta}{2}) + 2i\pi)\right] / \left[\sqrt{1-c\theta^2}(1-c\theta)\right]$.

$\lambda_{g_1}, \lambda_{g_2}, \lambda_H, \lambda_Z$	$O_{\varphi t}$	$O_{\varphi Q}^{(-)}$	$O_{t\varphi}$
$+,+,0,0$	$\frac{m_t^2\, v\, e\, g_s^2}{32\pi^2\, m_Z\, c_w\, s_w}\left[\log\left(\frac{s}{m_t^2}\right) - i\pi\right]^2$	$\frac{m_t^2\, v\, e\, g_s^2}{32\pi^2\, m_Z\, c_w\, s_w}\left[\log\left(\frac{s}{m_t^2}\right) - i\pi\right]^2$	$\frac{m_t\, v^2\, e\, g_s^2}{32\sqrt{2}\pi^2\, m_Z\, c_w\, s_w}\left[\log\left(\frac{s}{m_t^2}\right) - i\pi\right]^2$

Table 3: High energy behaviour of the $gg \to ZH$ helicity amplitudes with modified top-Z and top-Higgs interactions.

The top chromomagnetic operator O_{tG}, which modifies the top-gluon interactions, and $O_{\varphi G}$, which induces a contact interaction between the gluons and the Higgs bosons, both lead to growing amplitudes in multiple helicity configurations. In fact O_{tG} generates growing amplitudes in all helicity configurations, with a quadratic growth observed for the $(+-00)$ amplitude. However these growths are unlikely to impact LHC and HL-LHC observables as both coefficients are tightly constrained from global fits of collider data [9].

The top operators $O_{\varphi t}$, $O_{\varphi Q}^{(-)}$ and $O_{t\varphi}$, receive less stringent constraints from current measurements [9] and generate logarithmic growths in the $(++00)$ helicity configuration. This behaviour can be explained by considering the different diagrams these operators enter in. The operators $O_{\varphi t}$

and $O_{\varphi Q}^{(-)}$ modify the $t\bar{t}Z$ vertex, and also introduce a $t\bar{t}ZH$ vertex, with $O_{\varphi Q}^{(-)}$ adding a $b\bar{b}ZH$ vertex as well. The modified triangle diagrams with a Z propagator and with a $t\bar{t}ZH$ vertex cancel each other exactly such that the behaviour of the $O_{\varphi t}$ and $O_{\varphi Q}^{(-)}$ amplitudes can be understood from the SM box diagrams with a rescaled $t\bar{t}Z$ interaction. Boxes grow logarithmically when the two incoming gluons have the same polarisation and the Z boson is longitudinally polarised, and decrease in all other cases. Hence both operators lead to a logarithmic growth with energy in the $(++00)$ helicity configuration. In the SM this growth is not observed as the logarithmic terms coming from the box diagrams are cancelled exactly by the triangle diagrams. Furthermore, another consequence of the cancellation of the triangle diagrams in the presence of $O_{\varphi t}$ and $O_{\varphi Q}^{(-)}$ is that these operators exhibit the same behaviour as the top Yukawa operator $O_{t\varphi}$, which only enters in box diagrams where it rescales the $t\bar{t}H$ vertex. Thus, $gg \to ZH$ is only sensitive to the linear combination $c_{\varphi Q}^{(-)} - c_{\varphi t} + \frac{c_{t\varphi}}{y_t}$, where y_t is the top yukawa, and this degeneracy is exact and does not only hold in the high-energy limit.

3. The reach of $pp \to ZH$ at HL-LHC

The energy growths presented in the previous section motivate including the gluon-induced channel in a phenomenological analysis of ZH production to assess the sensitivity of this channel to poorly constrained third-generation operators. The quark-induced channel enters at tree-level and is sensitive to $O_{\varphi Q}^{(-)}$ and $O_{\varphi Q}^{(3)}$, while the gluon channel enters at NNLO and is sensitive to $O_{\varphi Q}^{(-)}$, $O_{\varphi t}$ and $O_{t\varphi}$. We extend a $q\bar{q} \to ZH$ analysis [10] to consider a $\mathrm{U}(2)_q \times \mathrm{U}(3)_d \times \mathrm{U}(2)_u \times (\mathrm{U}(1)_\ell \times \mathrm{U}(1)_e)^3$ flavour assumption and include the gluon-induced channel. We simulate the contribution of $gg \to ZH$ using `Madgraph5_aMC@NLO` and the `SMEFTatNLO` model [11] at LO in QCD for a centre-of-mass energy of 13 TeV and in the presence of one operator at a time. In our analysis strategy, we divide the simulated events into two categories, boosted and resolved, based on the presence of a boosted Higgs candidate or two resolved b-jets respectively. Additionally, the events are separated into two channels depending on whether zero or two charged leptons are present in the final state, and a binning is applied using $p_{T,\mathrm{min}} = \min\{p_T^Z, p_T^H\}$, with the bin boundaries optimised independently for each of the four categories.

The HL-LHC projected 95% C.L. bounds are presented in the left panel of Fig. 2. We assume SM-like measurements, uncorrelated observables and a systematic uncertainty of 5%. A first observation is that the operators entering in the quark-initiated process are more constrained than those only probed by the gluon-initiated channel. This is because $q\bar{q} \to ZH$ enters at tree-level and its contribution to the total cross-section is thus larger than the contribution of the gluon channel. We can compare the bounds coming from $pp \to ZH$ to bounds coming from global fits of collider data to assess the sensitivity of the $pp \to ZH$ process to third-generation operators. Global fits of LHC data constrain [9]:

$$c_{\varphi Q}^{(3)} \in [-0.69, 0.27]\ \mathrm{TeV}^{-2}, \qquad c_{\varphi t} \in [-15.6, 1.5]\ \mathrm{TeV}^{-2} \tag{3}$$

$$c_{\varphi Q}^{(-)} \in [-0.62, 1.29]\ \mathrm{TeV}^{-2}, \qquad c_{t\varphi} \in [-3.04, 3.53]\ \mathrm{TeV}^{-2} \tag{4}$$

Our HL-LHC projections are similar for $c_{\varphi Q}^{(3)}$ and $c_{\varphi Q}^{(-)}$. In the case of $c_{\varphi t}$, $pp \to ZH$ at HL-LHC sets a stronger negative bound than the current one but the positive bound is worse.

WC [TeV^{-2}]	95% C.L. Bound (5% syst.)
$c_{\varphi Q}^{(3)}$	[−0.72, 0.57]
$c_{\varphi Q}^{(-)}$	[−1.5, 1.1]
$c_{\varphi t}$	[−8.1, 19.6]
$c_{t\varphi}$	[−19.4, 8.0]

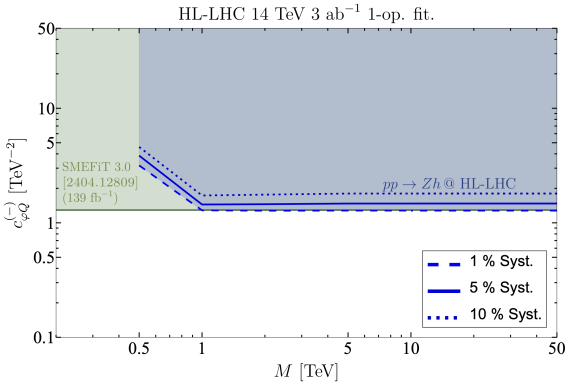

Figure 2: Left: Projected 95% C.L. bounds on $c_{\varphi Q}^{(-)}$ with different levels of systematic uncertainty at the HL-LHC from a one-operator fit as a function of the maximal-invariant-mass cut M. We also show the bound from the global fit to LHC data performed by the `SMEFiT` collaboration [9] with a dark green line. **Right:** Projected bounds at 95% C.L. from one-dimensional fits on the third-generation dimension-6 WCs probed by $pp \to ZH$ at HL-LHC with integrated luminosity of 3 ab^{-1}. The WCs are in units of TeV^{-2}.

Finally ZH production at HL-LHC is less competitive to probe $c_{t\varphi}$ as our projected bound is more than 4 times larger than the constraint from LHC data. Furthermore, we study the dependence of the HL-LHC projected bounds on the maximal invariant mass of the ZH system, M. The results are given in the right panel of Fig. 2 for $c_{\varphi Q}^{(-)}$, where the maximum absolute value of the projected bound is used. M acts as a proxy for the cutoff of the EFT, thus the HL-LHC projected bounds are valid as long as the cutoff of the EFT is $\gtrsim$ 1TeV, but they worsen considerably for lower cutoffs. Overall, ZH production offers good sensitivity to some top quark operators and could therefore have a significant impact when combined with other top quark production measurements in future global fits. The largest impact is expected for $c_{\varphi Q}^{(-)}$, to which $pp \to ZH$ is sensitive through both the quark and the gluon-initiated processes.

4. CP-violating top-Higgs interactions

Having considered the impact of CP-even SMEFT operators on gluon-induced ZH production, we now turn our attention to CP-violating effects. We start by extending the `SMEFTatNLO` model to include the relevant operators [12], which is achieved by implementing in the UFO the following ingredients:

- The Feynman rules for the vertices modified by the CP-violating operators.
- The Feynman rules for the rational terms R_2. These are needed within the Ossola-Papadopoulos-Pittau (OPP) reduction method [13], as implemented in `CutTools` allowing the automation of one-loop computations in `MadLoop` [14].
- The UV counterterms for the UV-divergent amplitudes.

Focusing on top-Higgs interactions, the top Yukawa operator gives rise to CP-violating effects when the imaginary part of its coefficient, denoted $\texttt{IM}c_{t\varphi}$, is non-vanishing. In $gg \to ZH$, $O_{t\varphi}$ enters only in the top-quark boxes shown in Fig. 1, and we implemented the modified CP-odd $t\bar{t}H$ Feynman rule in `SMEFTatNLO`. We calculated analytically the $ggZH$ R_2 contribution in the presence of $\texttt{IM}c_{t\varphi}$

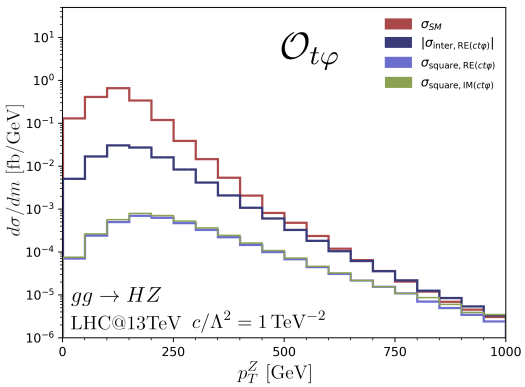

Figure 3: Differential cross-section of $gg \to ZH$ with respect to p_T^Z in the presence of $O_{t\varphi}$. The real part of the coefficient is denoted by $\texttt{RE}c_{t\varphi}$ and the imaginary part by $\texttt{IM}c_{t\varphi}$. Their square distributions overlap.

and found that it vanishes, and as $gg \to ZH$ is UV finite both in the SM and in the presence of $\texttt{IM}c_{t\varphi}$, not UV counterterm is needed.

Equipped with our modified version of `SMEFTatNLO`, we compared the impact of the CP-even and CP-odd parts of the Yukawa operator on the Z transverse momentum distribution, shown in Fig. 3. The interference of $\texttt{IM}c_{t\varphi}$ with the SM vanishes at the amplitude level. More specifically the individual helicity amplitudes have a non-zero interference with the SM, but these contributions cancel out with each other due to the CP properties of the helicity amplitudes. Furthermore, the square contributions of $\texttt{IM}c_{t\varphi}$ and $\texttt{RE}c_{t\varphi}$ overlap, which can be understood by examining the helicity amplitudes: the total amplitude is largely dominated by the $(++0\,0)$ helicity configuration, for which the $\texttt{RE}c_{t\varphi}$ and $\texttt{IM}c_{t\varphi}$ amplitudes have the same magnitude, leading to the observed overlapping distribution.

5. Conclusion

ZH production from gluon fusion is a useful process to probe deviations from the SM in the top quark sector. In particular this process is sensitive to CP-even and CP-odd SMEFT third-generation operators which lead to growing amplitudes in some helicity configurations. Combining the gluon and quark-induced channels in an analysis of ZH production gives competitive constraints on some third-generation operators, which motivates precision measurements of this process in future LHC runs and its inclusion in global fits.

References

[1] B. Grzadkowski, M. Iskrzynski, M. Misiak and J. Rosiek, *Dimension-Six Terms in the Standard Model Lagrangian*, *JHEP* **10** (2010) 085 [1008.4884].

[2] A. Rossia, M. Thomas and E. Vryonidou, *Diboson production in the SMEFT from gluon fusion*, *JHEP* **11** (2023) 132 [2306.09963].

[3] R. Mertig, M. Bohm and A. Denner, *FEYN CALC: Computer algebraic calculation of Feynman amplitudes*, *Comput. Phys. Commun.* **64** (1991) 345.

[4] V. Shtabovenko, R. Mertig and F. Orellana, *New Developments in FeynCalc 9.0*, *Comput. Phys. Commun.* **207** (2016) 432 [1601.01167].

[5] V. Shtabovenko, R. Mertig and F. Orellana, *FeynCalc 9.3: New features and improvements*, *Comput. Phys. Commun.* **256** (2020) 107478 [2001.04407].

[6] V. Shtabovenko, *FeynHelpers: Connecting FeynCalc to FIRE and Package-X*, *Comput. Phys. Commun.* **218** (2017) 48 [1611.06793].

[7] H. H. Patel, *Package-X: A Mathematica package for the analytic calculation of one-loop integrals*, *Comput. Phys. Commun.* **197** (2015) 276 [1503.01469].

[8] T. Hahn, *Generating Feynman diagrams and amplitudes with FeynArts 3*, *Comput. Phys. Commun.* **140** (2001) 418 [hep-ph/0012260].

[9] E. Celada, T. Giani, J. ter Hoeve, L. Mantani, J. Rojo, A. N. Rossia et al., *Mapping the SMEFT at high-energy colliders: from LEP and the (HL-)LHC to the FCC-ee*, *JHEP* **09** (2024) 091 [2404.12809].

[10] F. Bishara, P. Englert, C. Grojean, G. Panico and A. N. Rossia, *Revisiting $Vh(\to b\bar{b})$ at the LHC and FCC-hh*, *JHEP* **06** (2023) 077 [2208.11134].

[11] C. Degrande, G. Durieux, F. Maltoni, K. Mimasu, E. Vryonidou and C. Zhang, *Automated one-loop computations in the standard model effective field theory*, *Phys. Rev. D* **103** (2021) 096024 [2008.11743].

[12] M. O. A. Thomas and E. Vryonidou, *CP violation in loop-induced diboson production*, 2411.00959.

[13] G. Ossola, C. G. Papadopoulos and R. Pittau, *Reducing full one-loop amplitudes to scalar integrals at the integrand level*, *Nucl. Phys. B* **763** (2007) 147 [hep-ph/0609007].

[14] V. Hirschi, R. Frederix, S. Frixione, M. V. Garzelli, F. Maltoni and R. Pittau, *Automation of one-loop QCD corrections*, *JHEP* **05** (2011) 044 [1103.0621].

PoS(LHCP2024)129